

Seasonal Variability of Optical Properties in a Highly Turbid Lake (Laguna Chascomús, Argentina)

Gonzalo Luis Pérez*, María Eugenia Llamas, Leonardo Lagomarsino and Horacio Zagarese

Laboratorio de Ecología y Fotobiología Acuática, Instituto de Investigaciones Biotecnológicas, Instituto Tecnológico de Chascomús (IIB-INTECH), Provincia de Buenos Aires, Argentina.
Consejo Nacional de Investigaciones Científicas y Técnicas

Received 14 September 2010, accepted 1 February 2011, DOI: 10.1111/j.1751-1097.2011.00907.x

ABSTRACT

We study the underwater light field seasonality in a turbid lake, Laguna Chascomús (Buenos Aires, Argentina). We report (1) relationships between optical properties (OPs) and optically active substances (OASs); (2) relationships between inherent (IOPs) and apparent (AOPs) optical properties; and (3) the seasonal variability in OASs and OPs. Light absorption was dominated by the particulate fraction. The contributions of phytoplankton pigments and unpigmented components were similar. The best predictors of total particulate absorption, unpigmented particulate absorption, turbidity and vertical attenuation coefficient were total suspended solids or their ash content. Many OASs and OPs varied seasonally. The concentrations of OASs were higher during spring and summer, resulting in lower transparency and higher turbidity. However, mass-specific absorption coefficients displayed lower values during spring and summer. Thus, the higher light attenuation observed during spring and summer resulted from higher concentrations of relatively less absorptive OASs. Collectively, these results suggest that: (1) light extinction is enhanced during spring and summer; (2) the enhanced light extinction is due to changes in the particulate fraction; (3) the enhanced light extinction is mostly due to an increase in the amount of particulate material; and (4) the increase of particulate matter also enhanced light extinction through increased scattering.

INTRODUCTION

Underwater light penetration has paramount importance for aquatic ecosystems. From a fundamental perspective, the matching between the light requirements of primary producers and the amount and spectral quality of the underwater light field sets fundamental ecophysiological constraints to the development of the autotrophic community (1,2). Moreover, the concept of light availability is at the core of current ecological theory on the functioning of shallow lakes (3,4). From an applied point of view, a characterization of the underwater field provides valuable information on physico-chemical and biological processes, which may be used for monitoring water quality and assessing ecological condition (5–8).

Traditionally, water optics studies have been directed to four major goals: (1) predicting the propagation of underwater irradiance based on measurements of optically active substances (OASs) (9–12); (2) inferring the nature and concentration of OASs from *in situ* or remote measurements of apparent (AOPs) and/or inherent (IOPs) optical properties (13–16); (3) modeling light attenuation from IOPs measurements; and (4) inferring IOPs from measurements of light penetration with depth or from water-leaving radiance (17–22).

The optical characteristics of natural waters vary widely across ecosystems. The simplest systems (Case 1 waters) correspond to oligotrophic or ultraoligotrophic waters, in which the OPs are determined by the phytoplankton assemblage and its degradation products (23). Most water optics studies have focused on Case 1 waters, partly because they are typical of open ocean regions, which dominate global aquatic primary production, and also because they are simpler and more amenable to study than coastal, estuarine or inland waters (8,13,24,25). In contrast, the OPs of Case 2 waters are determined by a complex mixture of OASs, including not only algae-derived products, but also dissolved and particulate matter of mixed (*i.e.* autochthonous and allochthonous) origin. Inland waters are particularly complex. The OASs concentrations in lakes and rivers often exceed the limits found in marine waters (24,26), and may display large variability both, within and between water bodies, *e.g.* (8,27–30).

Laguna Chascomús is a large, hypereutrophic shallow lake. In this highly turbid environment, water transparency is mainly controlled by suspended material (31,32), and both phytoplankton and unpigmented particulate matter contribute similarly to total light absorption (33). Starting on June 2005, we undertook a detailed optical study of Laguna Chascomús. Our aim was to investigate the seasonal variability of the underwater light field. Here, we report (1) the relationship between OPs and the concentration of OASs; (2) the relationship between IOPs and AOPs; and (3) the seasonal variability in OASs, IOPs and AOPs. We also present field evidence on the role of external (weather and hydrological) forcing variables as drivers of the seasonal patterns of OPs.

MATERIALS AND METHODS

Study site and lake sampling. Laguna Chascomús (35°36'S, 58°02'W) is a large (area ~30 km²), shallow-lake (mean depth ~1.9 m) located in the Pampa region of Argentina. It belongs to the Salado river

*Corresponding author email: gperez@intech.gov.ar (Gonzalo Luis Pérez)
© 2011 The Authors
Photochemistry and Photobiology © 2011 The American Society of Photobiology 0031-8655/11

watershed, a large (801 km²) floodplain area with poorly developed drainage (average slope: 0.05%) (34). This hypereutrophic, turbid lake (33,35) is constantly mixed by persistent winds (31). The biotic community of Laguna Chascomús is rich and diverse, including hundreds of microbial (autotrophic and heterotrophic) species, zooplankton grazers and over 20 species of fish (36).

Laguna Chascomús was sampled every other week from June 2005 to September 2006. Water samples were collected at a central point of the lake and transported to the laboratory in 10 L polypropylene containers. Routine measurements of lake depth (*Z*), Secchi disk (*Sd*), water temperature (*T*) and dissolved oxygen concentration (using a YSI 5000 Meter) were performed *in situ* (see notation in Table S1).

Optically active substances. Total suspended solid (TSS) concentration was determined by weighing the dried residue (60°C) resulting from the filtration of a water sample through preirradiated and precombusted (530°C, 2 h) GF/F filters. Non-volatile particulate matter (also referred to as ash content, and abbreviated as Ash) was estimated by reweighing the GF/F filters after combustion at 530°C for 3 h (37). The ash-free dry weight (AFDW) was estimated as the difference between TSS and Ash. Dissolved organic carbon (DOC) was measured on filtered (GF/F ~0.7 µm) water samples using the high temperature Pt catalyst oxidation method (Shimadzu TOC-5000) following Sharp *et al.* (38). The instrument has a detection limit of 4 ppb of TOC and is routinely calibrated against a sodium phthalate standard. DOC analyses were performed by Dr. Don Morris at Lehigh University.

Inherent optical properties. Chromophoric dissolved organic matter (CDOM) absorption. The absorbance of CDOM was assessed by measuring the absorbance of filtered (0.22 µm) water samples from 380 to 750 nm, at 1 nm intervals. CDOM absorbance (A_{filtrate}) was measured in 0.01 m quartz cuvettes against an ultrapure water blank, using a Hitachi U-2000 spectrophotometer. According to Shooter *et al.* (39), the absorbance at 750 nm was assumed to be negligible. In order to minimize potential errors due to scattering, the values for each wavelength were corrected by subtracting the reading at 750 nm. The CDOM absorption coefficients [$ag(\lambda)$] were calculated as:

$$ag(\lambda) = \frac{2.303 \times A_{\text{filtrate}}(\lambda)}{r} \quad (1)$$

where $A_{\text{filtrate}}(\lambda)$ is the absorbance at λ and r is the cuvette path length in meters (1).

The spectral slope of CDOM absorption coefficients (S_g) for the 380–750 nm were obtained by nonlinear regression methods (40–42).

Particulate absorption. Absorption spectra by particles, $ap(\lambda)$, were determined using the filter-pad technique (43) on the material collected onto GF/F filters. In order to minimize light scattering, the wet filters were placed on the sensor end of the Hitachi U-2000 spectrophotometer, and measured against a blank clean filter, wetted with ultrapure water. The values were corrected by subtracting the reading at 750 nm, which were assumed to be negligible (39).

Absorption coefficients were estimated according to Mitchell and Kiefer (44):

$$ap(\lambda) = \frac{2.303 \times A_{\text{filter}}(\lambda) \times s}{V \times \beta(\lambda)} \quad (2)$$

where $A_{\text{filter}}(\lambda)$ is the absorbance of particulate matter on filter at λ , s is the clearance area of the filter, V is the water volume filtered and $\beta(\lambda)$ is the amplification factor vector calculated according to Bricaud and Stramski (45):

$$\beta(\lambda) = 1.63 \times A_{\text{filter}}(\lambda)^{-0.22} \quad (3)$$

Total absorption coefficients, $at(\lambda)$, were estimated as the sum of the absorption coefficients by particulates, dissolved matter and pure water:

$$at(\lambda) = ap(\lambda) + ag(\lambda) + aw(\lambda) \quad (4)$$

The absorption coefficients for pure water were taken from Kirk (1). Within the particulate fraction, we further distinguished between (1) the absorption due to within-cell (as opposed to extracted) chlorophyll and accessory photosynthetic pigments [hereinafter, phytoplankton absorption, $aph(\lambda)$] and (2) the absorption due to nonliving organic particles, inorganic particles and heterotrophic microorgan-

isms [hereinafter, unpigmented absorption, $ad(\lambda)$]. Two different methods have been proposed to estimate $ad(\lambda)$. The first method (46) is based on absorbance measurements performed after pigments extraction in absolute methanol. The second method (45) uses a mathematical approach to filter out the contribution of phytoplankton pigments to particulate absorption. The method estimates the absorption coefficients due to unpigmented particulate material, *i.e.* $ad(\lambda)$, by fitting a negative exponential function of λ to the total absorption spectra, *i.e.* $ap(\lambda)$, assuming that the ratios of phytoplankton absorption at specific wavelengths are known and constant [*i.e.* $aph(505)/aph(380) = 0.99$ and $aph(580)/aph(692.5) = 0.92$] [see Morrow *et al.* (47); Bricaud and Stramski (45); and Zhang *et al.* (48)]. Both methods estimate the absorption coefficients for phytoplankton, *i.e.* $aph(\lambda)$, as the difference between $ap(\lambda)$ and $ad(\lambda)$.

Although the estimates based on these two methods resulted statistically significantly different (paired *t*-test, $P < 0.05$, $n = 26$), the differences were virtually trivial in magnitude. In fact, the estimates based on Kishino *et al.* (46) produced estimates that, on average, were less than 5% higher than those obtained through the method by Bricaud and Stramski (45). Based on practical considerations, we opted for the method by Bricaud and Stramski (45). Hereinafter, $ad(\lambda)$ and $aph(\lambda)$ refer to mathematically derived estimates.

Chlorophyll *a* specific phytoplankton absorption coefficients, $aph^*(\lambda)$ were estimated as the quotient between $aph(\lambda)$ and T-Chl *a* (where T-Chl *a* stands for chlorophyll *a* + phaeophytin *a* concentration expressed in mg m⁻³). The mass specific absorption coefficients of total particulate and unpigmented particulate matter were calculated as $ap(\lambda)/\text{TSS}$ and $ad(\lambda)/\text{TSS}$, respectively. The effect of packaging on specific phytoplankton absorption was assessed by computing the dimensionless factor Q^*_a (49). Assuming a specific absorption coefficient for Chl *a* in solution of 0.0207 m² mg⁻¹ at 675 nm, $Q^*_a(675)$ was estimated as $aph^*(675)/0.0207$; after correcting $aph^*(675)$ for the presence of chl *b* or divinyl chl *b* (49).

The mean absorption coefficients within the photosynthetic active radiation (PAR) range (400–700 nm), $at(\text{PAR})$, $ag(\text{PAR})$, $ap(\text{PAR})$, $ad(\text{PAR})$, $aph(\text{PAR})$ and $aph^*(\text{PAR})$, were calculated as the arithmetic averages of monochromatic coefficients.

Nephelometric turbidity (as a proxy for scattering). Light scattering was indirectly assessed through measurements of nephelometric turbidity (T_n) (see [1] and references therein). We used a SCUFA (Turner[®]) submersible turbidimeter referenced to a bench-top 2100P (Hach[®]) turbidimeter calibrated against formazin liquid standards (Hach[®]).

Apparent optical properties. Spectral (380–750 nm) downward irradiance vertical profiles were performed using a USB2000 (Ocean Optics) spectroradiometer, attached to a fiber optic and a teflon diffuser. The measurements were performed around noon inside a black plastic container (50 × 50 × 40 cm) filled with freshly collected lake water. Water samples were gently shaken before measurements. This procedure was adopted in order to minimize errors due to waves. The magnitude of waves induced errors may be substantial in this highly turbid lake, where light is attenuated to less than 1% of incident irradiance within ~20 cm. Vertical diffuse attenuation coefficients for PAR, $K_d(\text{PAR})$ were determined from the slope of the linear regression of the natural logarithm of downward irradiances profiles vs depth. These values were validated by comparing the results against *in situ* $K_d(\text{PAR})$ estimates performed on calm days. No significant differences were obtained between the two methodologies (paired *t*-test, $P = 0.59$, $n = 15$).

A measure of the enhancement in vertical light extinction due to scattering was obtained by computing the ratio $K_d(\text{PAR})/K_{d_{\text{abs}}}(\text{PAR})$ (1,50), where:

$$K_{d_{\text{abs}}}(\text{PAR}) = \frac{at(\text{PAR})}{\cos\theta} \quad (5)$$

$K_{d_{\text{abs}}}(\text{PAR})$ is the vertical diffuse attenuation coefficient assuming negligible scattering, $at(\text{PAR})$ is the total absorption coefficient, and θ is the zenith angle of the light beam within the water (1). Moreover, for very turbid waters the angular structure of the light field becomes independent of the solar altitude [*i.e.* $K_{d_{\text{abs}}}(\text{PAR}) \sim at(\text{PAR})$] (19,51).

The mean irradiance in the water column ($I_{z, \text{mean}}$) was estimated following Ferrero *et al.* (52) as follows:

$$I_{z\text{mean}} = \frac{I_0 \times e^{-Kd(\text{PAR}) \times Z}}{Kd(\text{PAR}) \times Z} \quad (6)$$

where I_0 is the ground level mean daily irradiance (24 h), Kd (PAR) is the diffuse vertical attenuation coefficient for PAR, and Z is water column depth. The depth of the photic layer (Z_{eu}) was calculated as $4.6/Kd$ (PAR).

Phytoplankton community and pigments. Phytoplankton samples for qualitative analyses were collected with a 15- μm net and preserved in 4% formalin. Quantitative algal samples were preserved in PVC flasks with 1% acidified Lugol's iodine solution. Counts were performed according to Utermöhl (53). Replicate chambers were allowed to settle for a minimum of 24 h. A maximum counting error of 20% was accepted in estimating the abundance of each major algal group (54). In all cases individuals were counted, and for colonial or filamentous algae the size and/or number of cells corresponding to a standard individual was established. Phytoplankton biomass was estimated by calculating species biovolume following the criteria and formulae proposed by Hillebrand *et al.* (55).

Algal pigments were estimated from samples (110–250 mL) collected onto Whatman GF/F filters. Filters were immediately wrapped in aluminum foil and stored at -80°C . Pigments were extracted (overnight 4°C , in the dark, on a nitrogen-saturated atmosphere) using 90% vol/vol aqueous acetone and the extracts were cleared by centrifugation at 3000 rpm for 10 min. Pigment extracts were measured by ion pairing reverse-phase HPLC. The method applied has been described in detail by Laurion *et al.* (56), modified from Mantoura and Llewellyn (57). We used an Äkta basic chromatograph (Amersham, Buckinghamshire, UK), with a Phenomenex[®] Gemini C18 column (250 \times 4.6 mm, 5 μm), controlled by the program Unicorn (Amersham). For pigments identification and quantification we used standards from Sigma Inc. (Buchs, Switzerland) and from the International Agency for ^{14}C Determination. A few carotenoids for which no standards were available were identified based on published retention times (RT). In the absence of the corresponding standard, these carotenoids were quantified against fucoxanthin, or in the case of a myxoxanthophyll-like carotenoid, against myxoxanthophyll standards. This procedure did not allow the individualization of zeaxanthin and lutein, which are referred to as Zeax + Lut.

Weather variables. Solar radiation was recorded with a GUV 511 radiometer (Biospherical Instruments, Inc.) located in Buenos Aires city and an IL1700 radiometer (International Light) installed by the shore of Laguna Chascomús. Both radiometers are equipped with broadband PAR (400–750 nm) sensors.

Although the two radiometers are located about 100 km away from each other, if their measurements are averaged over several days (*i.e.* 6 days), they provide very similar and consistent mean daily irradiance estimates. In this work we use the data from the GUV 511 radiometer from which a more extended and uninterrupted data series was available.

Given that I_0 and W are highly variable on time scales of minutes, and considering that the system is likely to respond to average conditions (as opposed to instantaneous values), we assayed different time-windows for I_0 and W . For this purpose, we regressed the dependent variables [*e.g.* TSS, Sd, Kd (PAR), Tn] vs the mean irradiance calculated for a variable number of previous days (from 1 to 15 days) and mean wind speed calculated for a variable number of previous hours (from 1 to 24 h). We found that for incident solar radiation, the average daily fluence for the 6 days prior to sampling tended to produce the best fits (*i.e.* highest R^2). The mean ground level daily PAR irradiance (I_0) averaged over the 6 days prior to lake sampling is referred to as I_0 (6d). On the other hand, the mean wind speed averaged over the 9 h prior to sampling tended to produce the best fits and is referred to as W (9 h).

Statistical analyses. The relationships between OASs and OPs, as well as their temporal variation were analyzed using simple and multiple linear regressions. When multiple linear regressions were applied, stepwise backward procedure was performed in order to identify the variables that contributed the most to explain the variance in dependent variable. The occurrence of seasonality was assessed by two different statistical approaches. First, we compared values collected during the high radiation seasons (HRS, *i.e.* the austral spring and summer: from 21 September to 20 March) vs those collected during the low radiation seasons (LRS, *i.e.* the austral LRS: from 21

March to 20 September) using the *t*-test of means comparisons (or the Mann–Whitney rank sum test whenever the assumptions of normality were violated). In addition, the dependent variables were regressed against I_0 (6d), W (9 h), T and Z , and all their interaction terms. Regressions were made using stepwise multiple linear regression analysis, as described above. In regression models, we tested the normality (Kolmogorov–Smirnov test) and homoscedasticity (Spearman rank) assumptions. Multicollinearity was assessed by computing the variance inflation factors. Given the time series structure of the database, we also checked for potential autocorrelation of the residuals (Durbin–Watson test).

RESULTS

Optically active substances

Dissolved organic carbon concentration ranged from 15.46 to 20.22 mg L^{-1} , averaging $17.52 \pm 1.36 \text{ mg L}^{-1}$. TSS concentration varied widely from 75 to 630 mg L^{-1} , with a mean value of $243 \pm 143 \text{ mg L}^{-1}$. On average, the ash content represented ~65% of TSS. Total Chl *a* concentration ranged from 56.65 to 344.59 $\mu\text{g L}^{-1}$ (mean = $162.02 \pm 68.89 \mu\text{g L}^{-1}$). There was a significant, albeit weak, positive linear relationship between T-Chl *a* and TSS ($R^2 = 0.35$, $P < 0.001$, $n = 25$). The contribution of T-Chl *a* to TSS varied from 0.03% to 0.19%. Photosynthetic accessory pigments were identified as chlorophyll *b* (Chl *b*), chlorophyll e_2 (Chl *c*), neoxanthin (Neox), fucoxanthin (Fucox), an unidentified carotenoid (RT = 19.5 min, Carot 19.5), alloxanthin (Allox), myxoxanthophyll-like carotenoid (Myxo-like), zeaxanthin + lutein (Zeax + Lut), canthaxanthin (Canthax) and β -carotene (β -carot). The concentration of Zeax + Lut displayed a strong linear relationship with the Myxo-like carotenoid ($R^2 = 0.71$, $P < 0.05$, $n = 24$), but not with Chl *b*, suggesting that it is mostly composed by Zeax. The unidentified carotenoid (Carot 19.5) showed a strong linear relationship with Fucox ($R^2 = 0.93$, $P < 0.05$, $n = 24$). Overall, the composition of accessory pigments was dominated by Zeax + Lut, Fucox, Chl *b*, Carot 19.5, β -carot and Myxo-like carotenoid (in decreasing order), which together accounted for over 85% of total accessory pigment concentration.

The phytoplankton community was represented by 88 algal entities, including Chlorophyceae (38 taxa), Cyanobacteria (22 taxa), Bacillariophyceae (15 taxa), and less numerous representatives of the classes Zygothryx, Euglenophyceae, Xanthophyceae and Cryptophyceae (collectively referred to as other taxa). The algal community was mostly composed by Cyanobacteria colonies of small-cell *Aphanocapsa delicatissima*, co-occurring with filamentous Cyanobacteria (*i.e.* *Planktolyngbya contorta* and *Planktolyngbya limnetica*), small chlorococcales (*i.e.* *Monoraphidium spp.* and *Scenedesmus spp.*) and the diatom *Synedra berolinensis*. Cyanobacteria contributed 50% to total phytoplankton biovolume, followed by Chlorophyceae and Bacillariophyceae. Phytoplankton biovolume and cell density were highly correlated ($R = 0.81$, $P < 0.001$, $N = 23$). The T-Chl *a* and the accessory pigment cell content averaged 0.43 ± 0.21 and $0.24 \pm 0.11 \text{ pg cell}^{-1}$, respectively.

Inherent optical properties

CDOM absorption. Chromophoric dissolved organic matter absorption coefficients, a_g (PAR) and a_g (440), averaged 2.07 ± 0.53 and $4.65 \pm 0.91 \text{ m}^{-1}$, respectively (Fig. 1a). The

spectral slope of CDOM absorption spectra ranged from 0.009 to 0.019 nm⁻¹ (mean = 0.015 ± 0.003 nm⁻¹). No apparent relationship could be observed between *a_g* (PAR) and DOC concentration (*P* > 0.05) (Fig. 1b).

Particulate absorption. The absorption coefficients due to particulate matter, *a_p* (440) and *a_p* (PAR), averaged 15.44 ± 5.14 and 7.40 ± 2.52 m⁻¹, respectively, and dis-

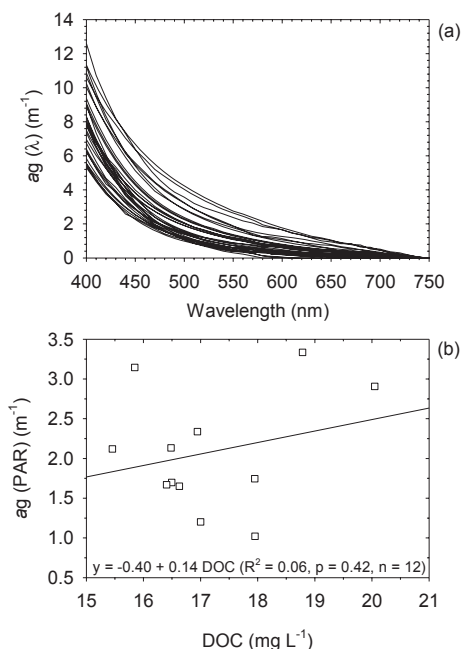


Figure 1. (a) Chromophoric dissolved organic matter spectral absorption coefficients [*a_g* (λ)]; (b) relationship between *a_g* (PAR) and dissolved organic carbon.

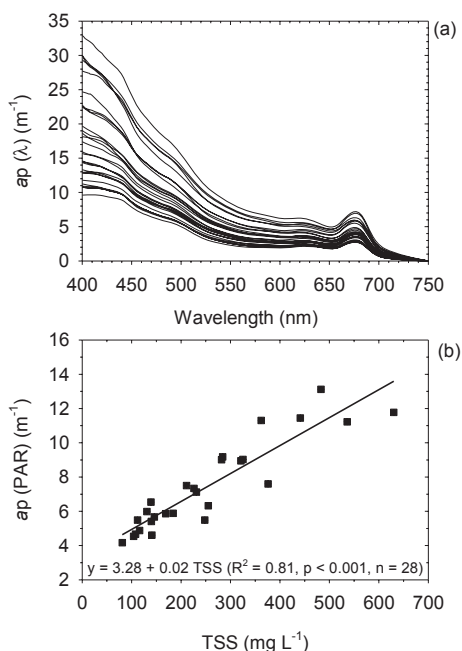


Figure 2. (a) Total particulate matter spectral absorption coefficients [*a_p* (λ)]; (b) linear relationship between *a_p* (PAR) and total suspended solids.

played a broad variation (*ca* three-fold) over the year. The *a_p* spectra are shaped by a blend of phytoplankton pigments and unpigmented particulate absorption (Fig. 2a). Strong linear relationships were found between particulate absorption coefficients and TSS. Roughly the 80% of the observed variation in absorption by particulates may be accounted for by the TSS concentration (Table 1, Fig. 2b). The ratios *a_p* (440)/TSS and *a_p* (PAR)/TSS averaged 0.071 ± 0.020 and 0.034 ± 0.009 m² g⁻¹, respectively.

Unpigmented absorption spectra displayed the characteristic exponential decreasing trend of absorption with increasing wavelengths (Fig. 3a). Values of unpigmented absorption, *a_d* (440) and *a_d* (PAR) averaged 9.66 ± 4.11 and 4.35 ± 1.82 m⁻¹, respectively, showing a broad variability (about 4.5-fold). Strong linear relationships were found between *a_d* (440) and *a_d* (PAR) vs the concentration of suspended particulate matter. TSS contributed to explain over 80% of the variance in *a_d*, but the ash content of TSS (Ash) explained an even greater (87%) percentage of the variance in

Table 1. Linear regression models for predicting optical properties (IOPs and AOPs) from optically active substances.

Predicted variables	Regression models	<i>n</i>	<i>R</i> ²	<i>P</i>
<i>a_p</i> (PAR)	Y = 3.28 + 0.02 TSS	28	0.81	<0.001
<i>a_p</i> (440)	Y = 7.01 + 0.03 TSS	28	0.81	<0.001
<i>a_d</i> (PAR)	Y = 1.72 + 0.01 Ash	28	0.87	<0.001
<i>a_d</i> (440)	Y = 3.74 + 0.03 Ash	28	0.87	<0.001
<i>a_{ph}</i> (675)	Y = 1.73 + 0.01 T-Chl <i>a</i>	22	0.79	<0.001
<i>a_{ph}</i> *(440)	Y = 2.62 T-Chl <i>a</i> ^{-0.84}	22	0.88	<0.001
<i>T_n</i>	Y = 47.1 + 0.99 Ash	30	0.87	<0.001
<i>T_n</i>	Y = 23.21 + 0.77 TSS	30	0.85	<0.001
<i>K_d</i> (PAR)	Y = 9.15 + 0.06 TSS	26	0.65	<0.001

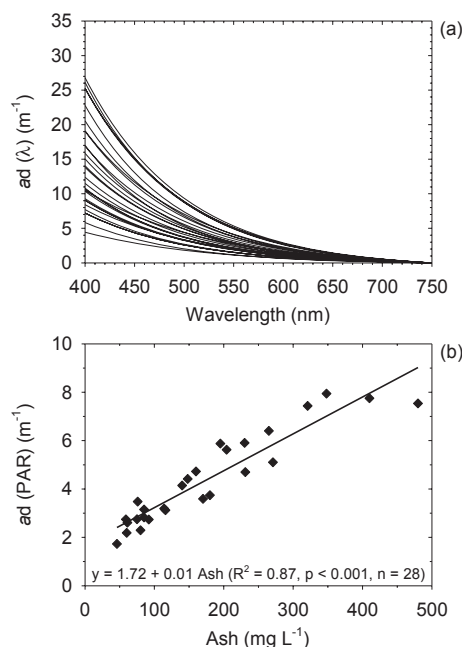


Figure 3. (a) Unpigmented particulate matter spectral absorption coefficients [*a_d* (λ)]; (b) linear relationship between *a_d* (PAR) and ash content (Ash).

ad (Table 1, Fig. 3b). The ratios ad (440)/TSS and ad (PAR)/TSS, averaged 0.042 ± 0.009 and $0.019 \pm 0.004 \text{ m}^2 \text{ g}^{-1}$, respectively, varying around 2.5-fold.

Phytoplankton absorption spectra were characterized by absorption peaks around 440, 490, 627 and 675 nm (Fig. 4a). The values of aph (440) and aph (675), corresponding to Chl a absorption maxima, averaged 5.44 ± 0.89 and $3.57 \pm 0.85 \text{ m}^{-1}$, respectively, and were linearly related to T-Chl a concentration. The observed variation in aph (675) was significant and linearly explained (79%) by changes in T-Chl a (Table 1, solid black circles in Fig. 4b). Total chlorophyll a specific phytoplankton absorption spectra showed substantial variability between samples (Fig. 5a). Values of $aph^*(440)$ averaged $0.036 \pm 0.012 \text{ m}^2 \text{ mg T-Chl } a^{-1}$, ranging from 0.021 to $0.056 \text{ m}^2 \text{ mg T-Chl } a^{-1}$ (about three-fold). The coefficient $aph^*(675)$ averaged $0.023 \pm 0.005 \text{ m}^2 \text{ mg T-Chl } a^{-1}$ and ranged from 0.016 to $0.032 \text{ m}^2 \text{ mg T-Chl } a^{-1}$ (about two-fold). Values of $aph^*(\lambda)$ displayed inverse nonlinear relationship with T-Chl a . For instance, $aph^*(440)$ decreased as a power function of T-Chl a (Table 1).

The specific phytoplankton absorption spectra normalized at 440 nm, $aph^*(\lambda)/aph^*(440)$, was much less variable (Fig. 5b). The ratio $aph^*(440)/aph^*(675)$ varied narrowly by a factor of about 1.6. However, the factor Q^*_a (675) varied between 0.37 and 0.84 (mean = 0.58 ± 0.16), about 2.3-fold, indicating that the package effect decreases absorption coefficients at 675 nm by 16–63%. On three samples dates, the Q^*_a (675) values exceeded the theoretical limit (*i.e.* higher than 1), and were therefore excluded from the analysis of phytoplankton absorption and related variables.

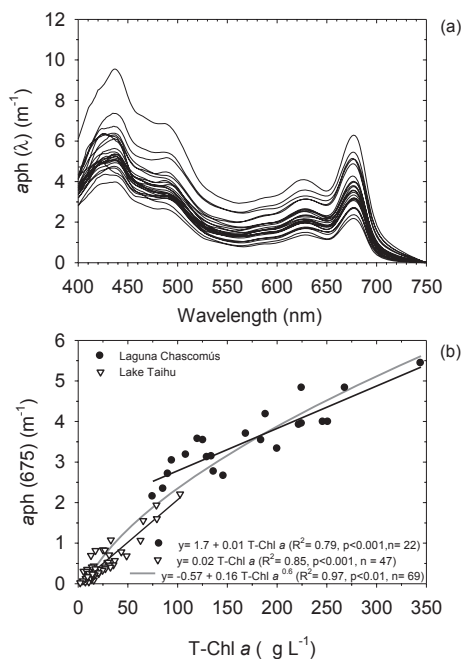


Figure 4. (a) Phytoplankton spectral absorption coefficients [$aph(\lambda)$]; (b) relationship between aph (675) and T-Chl a . Data from Laguna Chascomús are plotted as solid black circles; data from Lake Taihu (Le *et al.* 2009) were digitalized from the original publication and are plotted as open triangles. Linear fits for each individual lake are shown as solid black lines. The gray color curve is a power fit of the data for both lakes combined.

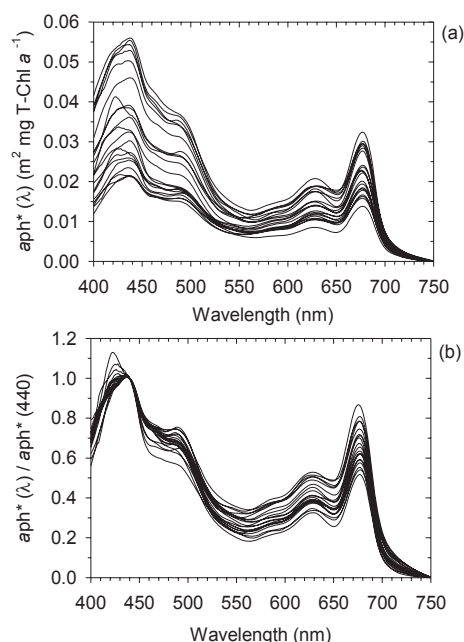


Figure 5. (a) Spectral T-Chl a specific phytoplankton absorption coefficients [$aph^*(\lambda)$]; (b) spectral T-Chl a specific phytoplankton absorption coefficients normalized at 440 nm.

Total absorption. Total absorption coefficients at (440) and at (PAR) averaged $20.11 (\pm 6.49)$ and $9.63 (\pm 2.68) \text{ m}^{-1}$, respectively. Examples of spectral absorption coefficients (400–700 nm) are shown in Fig. 6. Within the visible range, $at(\lambda)$ showed a steady decrease with increasing wavelengths, except for a small peak near the red end of the spectra. On average, the particulate fraction contributed over 77.9% to total absorption, while CDOM and the water itself contributed around 18.2% and 3.9%, respectively. Except for extremely windy days, the highest values of $at(\lambda)$ were observed during summer. The summer increase in $at(\lambda)$ was mostly due to an increase in the absorption by particulate matter, $ap(\lambda)$, (Fig. 6b,c).

Nephelometric turbidity

Nephelometric turbidity, T_n , ranged widely from 76.46 to 509.74 NTU, with an average of 209.18 ± 112.76 NTU. Between 85% and 88% of the variability in T_n may be accounted for by changes in TSS and Ash (Table 1). In contrast, T-Chl a , phytoplankton density and phytoplankton biovolume failed to explain the variability in T_n to any significant extent.

Apparent optical properties

Water transparency in Laguna Chascomús was remarkable low. Secchi disk readings (Sd) ranged from 0.06 to 0.17 m (mean = 0.11 ± 0.03 m). The vertical diffuse attenuation coefficient for PAR, K_d (PAR), averaged $22.76 \pm 7.40 \text{ m}^{-1}$. The values of K_d (PAR) were directly and significantly related to TSS, which explained about 65% of the observed variance (Table 1). Variation in K_d (PAR) was also significantly related to differences in turbidity ($R^2 = 0.69$, $P < 0.001$, $n = 26$). In contrast, T-Chl a did not significantly contribute to explain the

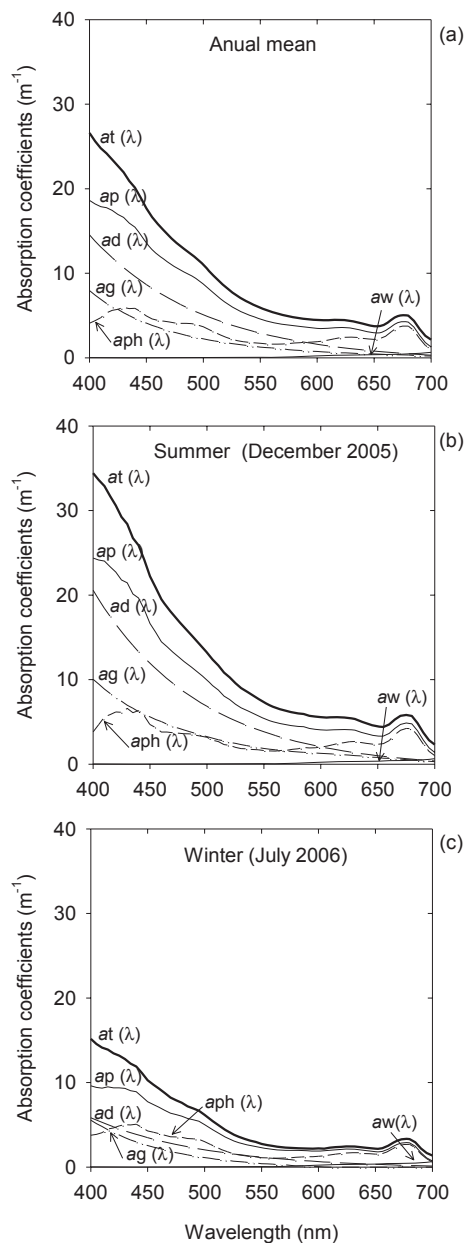


Figure 6. Total spectral absorption coefficients [$a_t(\lambda)$], and spectral absorption coefficient for CDOM [$a_g(\lambda)$], particulate matter [$a_p(\lambda) = [a_d(\lambda) + a_{ph}(\lambda)]$] and pure water [$a_w(\lambda)$]. (a) Annual average; (b) and (c) examples of a summer and a winter date, respectively.

variability in K_d (PAR). The estimated depth of the euphotic layer ranged from 0.13 to 0.44 m, and the ratio Z/Z_{eu} from 3.97 to 15.57. The mean PAR irradiance averaged over the whole water column, I_z , was low ($0.10\text{--}3.09\text{ W m}^{-2}$) and varied randomly over the year. The ratio K_d (PAR)/ $K_{d_{abs}}$ (PAR) averaged $2.25 \pm 0.20\text{ m}^{-1}$, suggesting that on average light scattering enhanced the vertical diffuse attenuation by roughly 114%.

Seasonal variation in OASs and OPs

Table 2 and Figure S1 summarize the trends observed in weather variables and lake depth. Solar radiation displayed the

Table 2. Weather and hydrological variables.

Variables	Mean \pm SD	Min.	Max.	V.C. (%)
I_0 (W m^{-2})	71.88 ± 42.92	6.98	161.61	59.71
I_0 (6d) (W m^{-2})	69.14 ± 38.65	19.85	148.10	55.90
W (km h^{-1})	9.84 ± 6.07	2.37	33.88	61.64
$W(9h)$ (km h^{-1})	7.75 ± 4.34	0.84	19.90	56.08
T ($^{\circ}\text{C}$)	14.81 ± 5.35	7.00	23.33	36.13
Z (m)	2.14 ± 0.14	1.88	2.33	6.66

marked seasonal trend typical of wet temperate regions. Mean daily PAR irradiance ranged from 6.98 to 161.61 W m^{-2} . Water temperature ranged from 7 to 23°C . The seasonal pattern of water temperature was essentially similar to that of solar radiation, except that it was smoother and slightly offset in time. The seasonal pattern of wind speed was less evident due to high day-to-day variations. Daily mean wind speed averaged 10 km h^{-1} , ranging from 2.37 to 33.88 km h^{-1} . The water column depth (Z) varied from 1.88 to 2.35 m (mean value of 2.14 m). A decreasing trend in depth was observed during study period.

Most OASs and OPs [*e.g.* TSS, Ash, $a_p(\lambda)$, $a_d(\lambda)$, T_n , K_d (PAR) and K_d (PAR)/ $K_{d_{abs}}$ (PAR)], as well as related variables (pigments concentration and pigments cell content) displayed significantly higher values during HRS than during LRS (Table 3). An obvious exception to this trend was S_d , which displayed higher values during LRS due to its inverse relationship with light extinction.

In contrast, none of variables related to the dissolved fraction showed significant differences between high and low radiation seasons. Similarly, no significant seasonal differences were observed for phytoplankton density, phytoplankton biovolume, phytoplankton absorption coefficients [$a_{ph}(\lambda)$] and pigment composition (relative to T-Chl a). Moreover, no significant differences in water column mean irradiance were observed. On the other hand, the absorption of particulate and unpigmented material per unit of mass [*i.e.* $a_p(\lambda)$ /TSS and $a_d(\lambda)$ /TSS] and the absorption of phytoplankton per unit of chlorophyll a [*i.e.* $a_{ph}^*(\lambda)$] displayed significantly lower values during HRS. The same trend was also observed for the factor Q^*_a (675) (Table 3).

Most variables that exhibited differences between LRS and HRS showed significant linear relationships with I_0 , suggesting that they track the natural variation of solar radiation (Table 4). TSS (Fig. 7) and phytoplankton pigments (Fig. 8b,c) appear to track the changes in incident solar radiation. Somehow unexpectedly, however, the algal density did not display significant differences between HRS and LRS (Fig. 8a). The time trend of additional optical variables are included in the online Supporting Information: total particulate matter [$a_p(\lambda)$], mass specific particulate absorption [a_p (PAR)/TSS] and the factor Q^*_a (Figure S2); nephelometric turbidity (Figure S3); and Secchi disk and K_d (PAR) (Figure S4).

Often, the data collected on two particularly windy days (labeled with # in the figures) departed from the general trends. Removing these two “outliers” typically improved the fit (Table 4). Including additional independent variables (*e.g.* wind speed, lake depth, temperature and interaction terms) into multiple linear regression models invariably increased the

Table 3. Average values calculated for the high radiation seasons (HRS) (spring and summer) and low radiation seasons (LRS) (fall and winter) for those variables that showed statistically significant differences (*t*-test, $P < 0.05$) between HRS and LRS.

Variables	LRS	HRS	<i>P</i> value
	Mean value	Mean value	
TSS (mg L ⁻¹)	186.32	323.67	0.006
Ash (mg L ⁻¹)	123.41	233.33	0.006
Ash/TSS (%)	61.75	70.67	0.004
T-Chl <i>a</i> (μg L ⁻¹)	125.97	207.89	0.006
Acc. pig. (μg L ⁻¹)	71.86	111.78	0.005
T-Pig. (μg L ⁻¹)	197.83	319.67	0.007
T-Chl <i>a</i> cell content (pg cell ⁻¹)	0.33	0.56	0.019
Acc. pig. cell content (pg cell ⁻¹)	0.19	0.30	0.019
<i>ap</i> (PAR) (m ⁻¹)	6.69	8.35	0.050
<i>ap</i> (440) (m ⁻¹)	13.97	17.40	0.027
<i>ad</i> (PAR) (m ⁻¹)	3.68	5.24	0.022
<i>ad</i> (440) (m ⁻¹)	8.18	11.62	0.026
<i>ad</i> (PAR)/ <i>ap</i> (PAR) (%)	53.87	61.96	<0.001
<i>ad</i> (440)/ <i>ap</i> (440) (%)	57.03	65.77	0.001
<i>ap</i> (PAR)/TSS (m ² g ⁻¹)	3.79×10^{-2}	2.85×10^{-2}	0.005
<i>ap</i> (440)/TSS (m ² g ⁻¹)	7.96×10^{-2}	5.93×10^{-2}	0.004
<i>ad</i> (PAR)/TSS (m ² g ⁻¹)	2.02×10^{-2}	1.73×10^{-2}	0.046
<i>ad</i> (440)/TSS (m ² g ⁻¹)	4.48×10^{-2}	3.83×10^{-2}	0.047
<i>aph</i> *(PAR) (m ² mg T-Chl <i>a</i> ⁻¹)	2.23×10^{-2}	1.58×10^{-2}	0.012
<i>aph</i> *(440) (m ² mg T-Chl <i>a</i> ⁻¹)	4.64×10^{-2}	3.03×10^{-2}	0.014
<i>aph</i> *(675) (m ² mg T-Chl <i>a</i> ⁻¹)	2.74×10^{-2}	1.99×10^{-2}	0.012
Q^*_a (675) (dimensionless)	0.76	0.50	0.003
<i>Tn</i> (NTU)	166.29	273.51	0.008
<i>Sd</i> (m)	0.12	0.09	0.012
<i>Kd</i> (PAR) (m ⁻¹)	19.86	28.22	0.004
<i>Kd</i> (PAR)/ <i>Kd</i> _{abs} (PAR)	2.21	2.52	0.035

proportion of explained variance, suggesting that, in addition to incident light, other variables may be important in controlling OAs and OPs.

DISCUSSION

Laguna Chascomús is a highly turbid and optically complex water system. The values of total absorption, nephelometric turbidity and light attenuation are remarkably high. To the best of our knowledge, very few studies have reported comparable values. V.-Balogh *et al.* (58) reported *Kd* (PAR) values of 23 m⁻¹ for one of the studied water bodies in Hungary; and Kirk (1) reported *Kd* (PAR) as high as 25 m⁻¹ in Lake George (Australia). These are among highest values ever documented. In Laguna Chascomús *Kd* (PAR) values often exceeded 30 m⁻¹, reaching a maximum of 36.16 m⁻¹. In addition, the very high total absorption coefficients (~9 m⁻¹) for PAR range and (~13 m⁻¹) at 440 nm reported for Lake Taihu (China) (59,60), are roughly half as large as those measured in Laguna Chascomús. Light scattering (estimated as nephelometric turbidity) also showed high values. Nephelometric turbidity measured in Laguna Chascomús lay within the range reported for the highly turbid Lake Carl Blackwell (16-1140 NTU) by Nolen *et al.* (28). All the previous examples are optically complex systems and exceptionally turbid environments.

In a previous study, we reported that in Laguna Chascomús the absorption of incident PAR was largely dominated by particulate matter (33). Here, we confirmed that, despite high absorption coefficients due to CDOM (*ag*), particulate fraction (*ap*) has a prominent role in light absorption. Within the latter fraction, both phytoplankton pigments (*aph*) and unpigmented (*ad*) components contributed similarly to particulate absorption (Fig. S2a). Zhang and coauthors also reported similar contributions of both fractions to *ap* (48,59). High particulate absorption coefficients and similar partitioning between *aph* and *ad* are frequent traits of many turbid lakes and estuaries (1,8,15,48,61). The similarity of *aph* and *ad* values represents an important obstacle for remote sensing efforts to estimate OASs (14,25,48,62) and analysis of cell size and community structure (63).

In Laguna Chascomús, the best predictors of total particulate absorption (*ap*), unpigmented particulate absorption (*ad*), turbidity (*Tn*) and vertical attenuation coefficient [*Kd* (PAR)] were either TSS or the ash content (Table 1). It was only after removing the effect of unpigmented particulate matter, that chlorophyll *a* (T-Chl *a*) became the best predictor of phytoplankton absorption. The relationship between *aph* (675) and T-Chl *a* obtained in this study spans the highest range of chlorophyll *a* concentrations (from 70 to 355 μg L⁻¹) published so far. The fitted line has a non-zero intercept, which may partly result from the particular phytoplankton composition, which includes many Chlorophyceae species (Fig. 8a). In fact, correcting for the presence of Chl *b* to phytoplankton absorption at 675 nm decreased the intercept by roughly a half. Nevertheless, the rate at which *aph* (675) increases with increasing T-Chl *a* is lower than that found by other authors (62,64). Decreases in chlorophyll *a* specific absorption at high chlorophyll *a* concentrations have been previously reported. Plotting our own data together with those reported by Le *et al.* (62) results in a slightly curvilinear relationship (Fig. 4b) similar to the power functions described (49,64,65).

We have previously reported that the concentration of TSS in Laguna Chascomús tends to track the seasonal variation in incident solar radiation (31,32,66). Using outdoor mesocosms filled with water from Laguna Chascomús, we were also able to experimentally demonstrate that TSS and turbidity increased with the amount of incident solar radiation (67). In addition, several other optical variables [*i.e.* *Kd* (PAR), *ad*, *ap*/TSS] showed the similar trends (either positive or negative) with irradiance than that observed in the lake (G. L. Pérez, unpublished). In this study, we have shown that many OASs and optical properties varied seasonally in Laguna Chascomús (Tables 3 and 4). As a general rule, the concentrations of OASs were higher during the HRS, which translated into high light absorption, lower transparency and higher turbidity. However, several mass-specific (*ap*/TSS and *ad*/TSS) and chlorophyll *a*-specific (*aph**) absorption coefficients, as well as the Q^*_a quotient displayed lower values during HRS than during LRS. In other words, the higher light attenuation observed during HRS resulted from higher concentrations of relatively less absorptive OASs. Scattering is another important component of light attenuation. The contribution of scattering to *Kd* (PAR) was higher during HRS than during LRS. Scattering (estimated as nephelometric turbidity) was strongly related to TSS and Ash, but was unrelated T-Chl *a* and phytoplankton

Table 4. Summary of the regression model analyses investigating potential relationships between optically active substances and optical properties vs weather and hydrological variables.

Dependent variables	Irradiance fixed model			Best regression model		
	Variable	R^2	n	Variables	R^2	n
TSS	+ I_0 (6d)	0.33 0.44	29 27	+ I_0 (6d) + W (9h) + [I_0 (6d) W (9h)]	0.68 0.76	28 26
Ash	+ I_0 (6d)	0.31 0.42	29 27	+ I_0 (6d) + W (9h) + [I_0 (6d) W (9h)]	0.67 0.65	28 26
Ash/TSS (%)	+ I_0 (6d)	0.26 0.34	29 27	+ Z + [I_0 (6d) W (9h)] + Z + [I_0 (6d) W (9h)]	0.62 0.63	27 25
T-Chl a	+ I_0 (6d)	0.43 0.45	25 23	+ [I_0 (6d) W (9h)] + [I_0 (6d) W (9h)]	0.49 0.52	25 23
Accessory pigments	+ I_0 (6d)	0.36 0.37	25 23	+ [I_0 (6d) W (9h)] + [I_0 (6d) W (9h)]	0.49 0.52	25 23
Total pigments	+ I_0 (6d)	0.41 0.44	25 23	+ [I_0 (6d) W (9h)] + [I_0 (6d) W (9h)]	0.51 0.52	25 23
T-Chl a cell content	+ I_0 (6d)	0.52 0.50	18 16	+ I_0 (6d) + [I_0 (6d) W (9h)]	0.52 0.50	18 16
Acc. pig. cell content	+ I_0 (6d)	0.46 0.45	18 16	+ [I_0 (6d) W (9h)] + [I_0 (6d) W (9h)]	0.51 0.53	18 16
ap (PAR)	+ I_0 (6d)	0.23 0.48	28 26	+ I_0 (6d) + W (9h) + [I_0 (6d) W (9h)]	0.59 0.63	27 25
ap (440)	+ I_0 (6d)	0.24 0.50	28 26	+ I_0 (6d) \times W (9h) + [I_0 (6d) W (9h)]	0.51 0.64	27 25
ad (PAR)	+ I_0 (6d)	0.32 0.53	28 26	+ I_0 (6d) + W (9h) + [I_0 (6d) W (9h)]	0.65 0.70	27 25
ad (440)	+ I_0 (6d)	0.32 0.53	28 26	+ I_0 (6d) + W (9h) + [I_0 (6d) W (9h)]	0.64 0.63	27 25
ad (PAR)/ ap (PAR) (%)	+ I_0 (6d)	0.39 0.42	28 26	+ Z + [I_0 (6d) W (9h)] + Z + [I_0 (6d) W (9h)]	0.64 0.64	27 25
ad (440)/ ap (440) (%)	+ I_0 (6d)	0.34 0.38	28 26	+ Z + [I_0 (6d) W (9h)] + Z + [I_0 (6d) W (9h)]	0.65 0.65	27 25
ap (PAR)/TSS	- I_0 (6d)	0.32 0.38	27 25	- I_0 (6d) - W (9h) - I_0 (6d) - W (9h)	0.55 0.55	26 24
ap (440)/TSS	- I_0 (6d)	0.31 0.36	27 25	- I_0 (6d) - W (9h) - I_0 (6d) - W (9h)	0.56 0.55	26 24
ad (PAR)/TSS	- I_0 (6d)	0.17 0.20	28 26	- [I_0 (6d) W (9h)] - [I_0 (6d) W (9h)]	0.33 0.33	27 25
ad (440)/TSS	- I_0 (6d)	0.16 0.19	28 26	- [I_0 (6d) W (9h)] - [I_0 (6d) W (9h)]	0.32 0.31	27 25
aph^* (PAR)	- I_0 (6d)	0.25 0.24	25 23	- I_0 (6d) - [I_0 (6d) W (9h)]	0.25 0.26	25 23
aph^* (440)	- I_0 (6d)	0.26 0.24	25 23	- I_0 (6d) - [I_0 (6d) W (9h)]	0.26 0.26	25 23
aph^* (675)	- I_0 (6d)	0.22 0.21	25 23	- I_0 (6d) - [I_0 (6d) W (9h)]	0.22 0.23	25 23
Q^*_a (675)	- I_0 (6d)	0.29 0.27	25 23	- I_0 (6d) - Z - I_0 (6d)	0.29 0.37	25 23
T_n	+ I_0 (6d)	0.36 0.49	30 28	+ [I_0 (6d) W (9h)] + [I_0 (6d) W (9h)]	0.68 0.73	29 27
S_d	- I_0 (6d)	0.33 0.48	28 26	- I_0 (6d) - W (9h) - Z - [I_0 (6d) W (9h)]	0.59 0.64	27 24
K_d (PAR)	+ I_0 (6d)	0.34 0.38	26 24	+ [I_0 (6d) W (9h)] + [I_0 (6d) W (9h)]	0.45 0.44	25 23

The left side of the table corresponds to single linear regression models with incident irradiance as the only independent variable. The right side of the table corresponds to the best multiple linear regression models obtained through a backward stepwise variable selection method. For each dependent variable, the top row corresponds to models including all data points, while the bottom row (in bold lettering and dim gray background) displays the results after deleting two potential outliers (*i.e.* very windy days). The + and - symbols indicate positive and negative effects respectively.

density. These results suggest that the non-algal components of the microbial community (*i.e.* nonliving organic matter, inorganic matter and heterotrophic microorganisms) are responsible for scattering in general, and for the enhancement of the scattering during HRS in particular. Collectively, these results suggest that: (1) light extinction is enhanced during the high radiation season; (2) the enhanced extinction of light is

due to changes occurring within the particulate fraction; (3) the enhanced extinction of light is mostly due to an increase in the amount of particulate material, which counteracts (actually, overcompensates for) the decrease in the mass-specific absorption of suspended solids; and (4) the increase of particulate matter also enhanced light extinction through increased scattering.

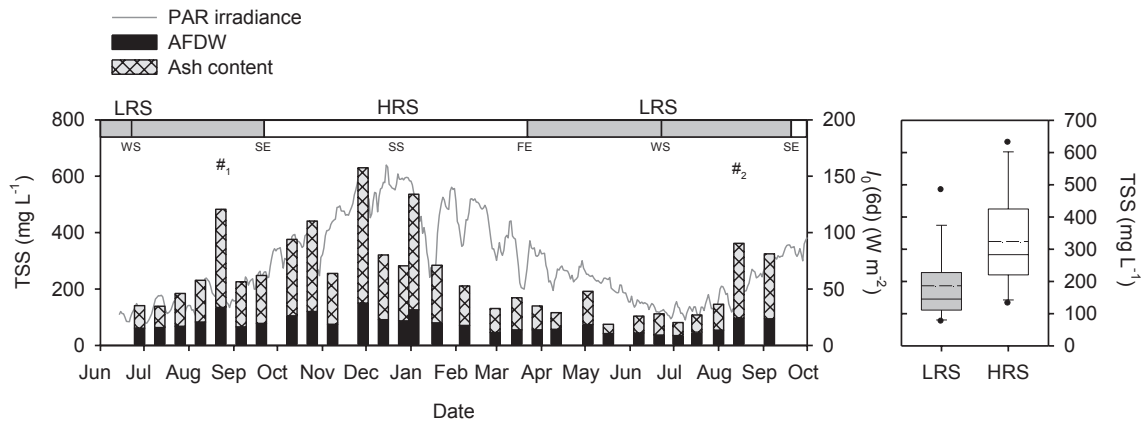


Figure 7. Left panel: Seasonal variation in total suspended solid (TSS). The two fractions of TSS (Ash and AFDW) are distinguished by different fill patterns. The I_0 (6d) PAR irradiance is plotted in gray line as a reference. HRS: high radiation seasons (spring and summer), LRS: low radiation season (fall and winter), WS: winter solstice, SE: spring equinox, SS: summer solstice, FE: fall equinox. Two particularly windy days ($\sim 17 \text{ km h}^{-1}$) are labeled as #1 and #2. Right panel: box plots of TSS concentration for the LRS and HRS.

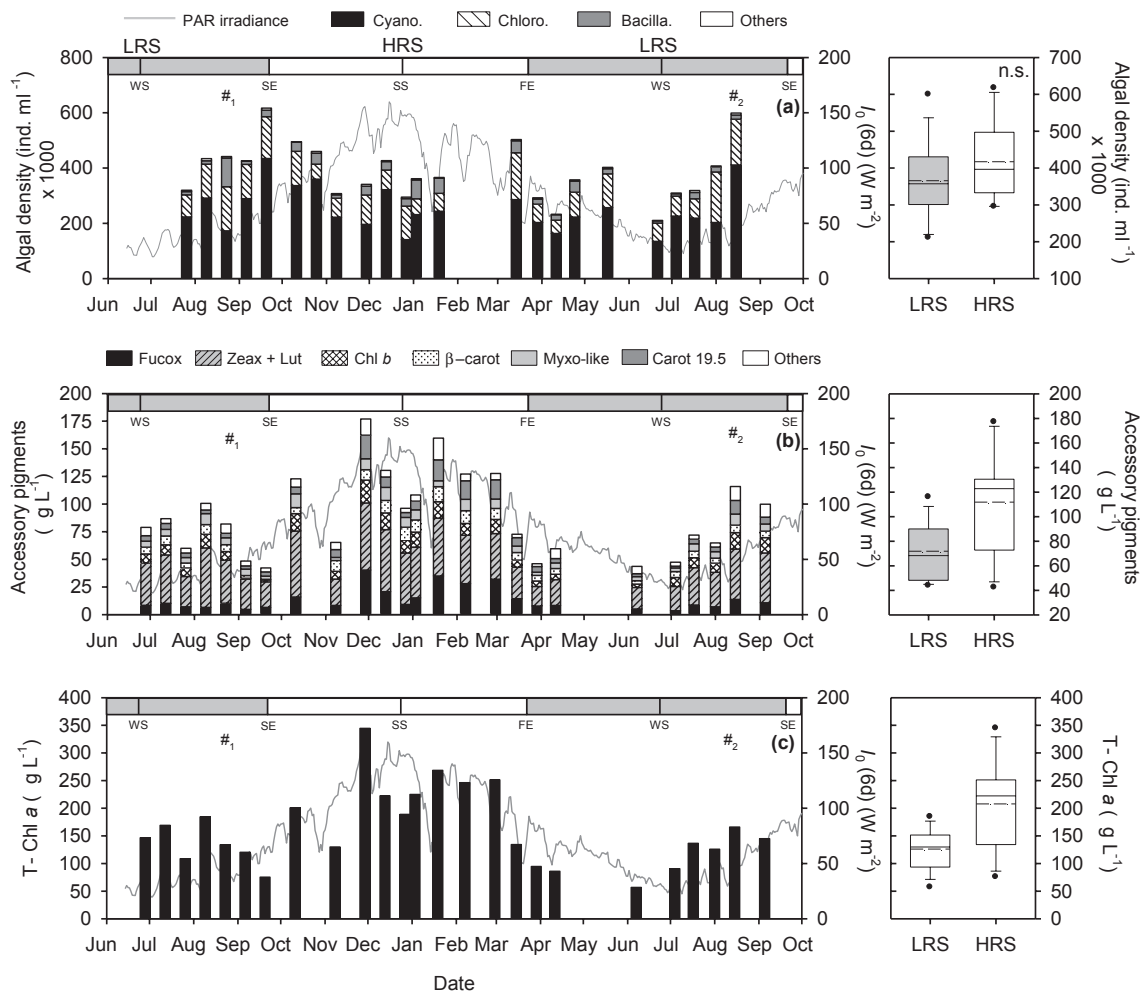


Figure 8. Left panels: seasonal variation in (a) algal density, (b) accessory pigments, (c) T-Chl *a*. Right panels: box plots of each variable for the low radiation season and high radiation seasons. n.s. (not statistically significant). All other references as in Fig. 7.

In the previous paragraphs, we discussed the role of incident solar radiation in controlling OASs and OPs by comparing their behavior during HRS vs LRS. Moreover, the effect of

light on the OASs and OPs may be inferred from the regression analyses summarized in Table 4, showing that most variables displayed statistically significant relationships with I_0 (6d).

These latter analyses are perhaps more comprehensive, as they also take into account additional external forcing variables. In fact, the amount of total variance explained by the regression models almost invariably increased if and when additional variables (*i.e.* wind speed and lake depth, and interaction terms) were included in the regression models. Moreover, the amount of total variance explained by I_0 (6d) increased when two particularly windy days were excluded from the regression model, suggesting that the resuspension of heavier material, which generally rests on the lake bottom, may occasionally be a major source of turbidity. The inclusion of Z explaining some studied variables may be related with the interaction between sediment resuspension and biogenesis production of suspended particles. Under light-limited conditions, suspended particles concentration and water transparency is expected to be related to mixing depth (68,31). In addition, the relationship between wave amplitude and lake depth is critical to predict the extent of sediment resuspension (69,70).

Despite the remarkable seasonality of several OASs and OPs, the phytoplankton community structure (Fig. 8a) and pigment composition remained fairly unchanged over the year. Such stability is consistent with the limited variability in phytoplankton spectral shape (Fig. 5b). Actually, the observed variability in aph^* appears to be related to the changes in the extent of pigment packaging (Q^*_a). In fact, the package effect could account for the 63% decrease in absorption coefficients, $aph^*(675)$, observed in summer. Increased pigment packaging may result from increases in either cell size or in cell pigment concentration (71). Given that the phytoplankton community structure remained fairly constant over the year, the enhancement of the package effect in summer is likely a consequence of the higher cell pigment content observed during the HRS.

In this highly turbid lake, phytoplankton primary production is constantly limited by light availability (32,35). The availability of light is mainly controlled by high light absorption and scattering by particulate matter, whose amount and optical properties are strongly affected by the incident light. Interesting, and somehow counter-intuitively, the major process controlling light availability is not phytoplankton self-shading, but the depletion of radiant energy caused by absorption and scattering due to non-algal particulates (*i.e.* background light attenuation). Phytoplankton competition with non-algal particles is well known in many coastal and estuarine environments (72,73). Most light-limited water column models (68,74) incorporate the background light attenuation as a baseline unrelated to light input. In Laguna Chascomús, however, the collected evidence suggests that the non-algae particulate matter dynamics is driven, to a large extent, by the amount of incident light. We therefore suspect that the non-algae particulate matter corresponds to heterotrophic components that develop at the expense of phytoplankton primary production.

Acknowledgements—We thank Dr. Yunlin Zhang for his advice on solving the system of equations for calculating unpigmented absorption coefficients, Dr. Don Morris for TOC analyses and J. Bustingorry and R. Escaray for field and lab assistance. This work was supported by Agencia Nacional de Promoción Científica y Tecnológica, PICT07-429 and by Consejo Nacional de Investigaciones Científicas y Técnicas, PIP-01301.

SUPPORTING INFORMATION

Additional Supporting information may be found in the online version of this article:

Figure S1. Time trends of (a) ground level par irradiance and temperature, (b) mean wind speed and (c) lake depth.

Figure S2. Left panels: seasonal variation in (a) total particulate matter [$ap(\lambda)$], (b) mass specific particulate absorption [$ap(\text{PAR})/\text{TSS}$] and (c) the dimensionless factor Q^*_a . Right panels: box plots of each variable for the LRS and HRS. The I_0 (6d) PAR irradiance is plotted in gray line as a reference. HRS = high radiation seasons (spring and summer); LRS = low radiation season (fall and winter); WS = winter solstice; SE = spring equinox; SS = summer solstice; FE = fall equinox.

Figure S3. Left panel: seasonal variation in nephelometric turbidity (T_n). Right panel: box plots of turbidity for the LRS and HRS. All other references as in Fig. S2.

Figure S4. Left panels: seasonal variation in (a) Secchi disk (S_d) and (b) K_d (PAR). Right panels: box plots of each variable for the LRS and HRS. All other references as in Fig. S2.

Table S1. Abbreviations of terms and variables used in the text.

Please note: Wiley-Blackwell are not responsible for the content or functionality of any supporting materials supplied by the author. Any queries (other than missing materials) should be directed to the corresponding author for the article.

REFERENCES

- Kirk, J. T. O. (1994) *Light and Photosynthesis in Aquatic Ecosystems*. Cambridge University Press, Cambridge.
- Stomp, M., J. Huisman, F. de Jongh, A. J. Veraart, D. Gerla, M. Rijkeboer, B. W. Ibelings, U. I. A. Wollenzien and L. J. Stal (2004) Adaptive divergence in pigment composition promotes phytoplankton biodiversity. *Nature* **432**, 104–107.
- Scheffer, M., S. H. Hosper, M. L. Meijer, B. Moss and E. Jeppesen (1993) Alternative equilibria in shallow lakes. *Trends Ecol. Evol.* **8**, 275–279.
- Scheffer, M. and E. H. Van Nes (2007) Shallow lakes theory revisited: Various alternative regimes driven by climate, nutrients, depth and lake size. *Hydrobiologia* **584**, 455–466.
- Tegler, B., M. Sharp and M. A. Johnson (2001) Ecological monitoring and assessment network's proposed core monitoring variables: An early warning of environmental change. *Environ. Monit. Assess.* **67**, 29–56.
- Gallegos, C. L. (2001) Calculating optical water quality targets to restore and protect submersed aquatic vegetation: Overcoming problems in partitioning the diffuse attenuation coefficient for photosynthetically active radiation. *Estuaries* **24**, 381–397.
- Lowe, E. F., L. E. Battoe, M. F. Coveney, C. L. Schelske, K. E. Havens, E. R. Marzolf and K. R. Reddy (2001) The restoration of Lake Apopka in relation to alternative stable states: An alternative view to that of Bachmann *et al.* (1999). *Hydrobiologia* **448**, 11–18.
- Reinart, A., B. Paavel, D. Pierson and N. Strömbeck (2004) Inherent and apparent optical properties of Lake Peipsi, Estonia. *Boreal Environ. Res.* **9**, 429–445.
- Morris, D. P., H. Zagarese, C. E. Williamson, E. G. Balseiro, B. R. Hargreaves, B. Modenutti, R. Moeller and C. Queimalinos (1995) The attenuation of solar UV radiation in lakes and the role of dissolved organic carbon. *Limnol. Oceanogr.* **40**, 1381–1391.
- LaPerriere, J. D. and J. A. Edmundson (2000) Limnology of two lake systems of Katmai National Park and Preserve, Alaska:

- Part II. Light penetration and Secchi depth. *Hydrobiologia* **418**, 209–216.
11. Zhang, Y., B. Zhang, R. Ma, S. Feng and C. Le (2007) Optically active substances and their contributions to the underwater light climate in Lake Taihu, a large shallow lake in China. *Fundam. Appl. Limnol.* **170**, 11–19.
 12. Xu, J., R. Hood and S.-Y. Chao (2005) A simple empirical optical model for simulating light attenuation variability in a partially mixed estuary. *Estuaries and Coasts* **28**, 572–580.
 13. Gallegos, C. L., D. L. Correll and J. W. Pierce (1990) Modeling spectral diffuse attenuation, absorption, and scattering coefficients in a turbid estuary. *Limnol. Oceanogr.* **35**, 1486–1502.
 14. Gons, H. J. (1999) Optical teledetection of chlorophyll a in turbid inland waters. *Environ. Sci. Technol.* **33**, 1127–1132.
 15. Gallegos, C. L. (2005) Optical water quality of a blackwater river estuary: The lower St. Johns River, Florida, USA. *Estuar. Coast. Shelf. Sci.* **63**, 57–72.
 16. Raaj, R., M. Ramalingam, S. K. Ghosh and U. C. Kothiyari (2008) Mapping of suspended sediments using site specific seasonal algorithms. *J. Indian Soc. Remote Sens.* **36**, 61–68.
 17. Kirk, J. T. O. (1984) Dependence of relationship between inherent and apparent optical properties of water on solar altitude. *Limnol. Oceanogr.* **29**, 350–356.
 18. Weidemann, A. D. and T. T. Bannister (1986) Absorption and scattering coefficients in Irondequoit Bay. *Limnol. Oceanogr.* **31**, 567–583.
 19. Kirk, J. T. O. (1994) Characteristics of the light field in highly turbid waters: A Monte Carlo study. *Limnol. Oceanogr.* **39**, 702–706.
 20. Mobley, C. D. (1994) *Light and Water: Radiative Transfer in Natural Waters*. Academic Press, San Diego, CA.
 21. Belzile, C., J. A. E. Gibson and W. F. Vincent (2002) Colored dissolved organic matter and dissolved organic carbon exclusion from lake ice: Implications for irradiance transmission and carbon cycling. *Limnol. Oceanogr.* **47**, 1283–1293.
 22. Albert, A. and C. D. Mobley (2003) An analytical model for subsurface irradiance and remote sensing reflectance in deep and shallow case-2 waters. *Optics Express*. **11**, 2873–2890.
 23. Morel, A. and L. Prieur (1977) Analysis of variations in ocean color. *Limnol. Oceanogr.* **22**, 709–722.
 24. Reinart, A., A. Herlevi, H. Arst and L. Sipelgas (2003) Preliminary optical classification of lakes and coastal waters in Estonia and south Finland. *J. Sea Res.* **49**, 357–366.
 25. Tyler, A. N., E. Svab, T. Preston, M. Présing and W. A. Kovács (2006) Remote sensing of the water quality of shallow lakes: A mixture modelling approach to quantifying phytoplankton in water characterized by high-suspended sediment. *Int. J. Remote Sens.* **27**, 1521–1537.
 26. Reinart, A. and K. Valdmets (2007) Variability of optical water types in Lake Peipsi. *Proc. Est. Acad. Sci. Biol. Ecol.* **56**, 33–46.
 27. Kirk, J. T. O. (1980) Spectral absorption properties of natural waters: Contribution of the soluble and particulate fractions to light absorption in some inland waters of south-eastern Australia. *Aust. J. Mar. Freshwater Res.* **31**, 287–296.
 28. Nolen, S. L., J. Wilhm and G. Howick (1985) Factors influencing inorganic turbidity in a great plains reservoir. *Hydrobiologia* **123**, 109–117.
 29. Pérez, G. L., C. P. Queimaliños and B. E. Modenutti (2002) Light climate and plankton in the deep chlorophyll maxima in North Patagonian Andean lakes. *J. Plankton Res.* **24**, 591–599.
 30. Paavel, B., H. Arst and A. Reinart (2008) Variability of bio-optical parameters in two North-European large lakes. *Hydrobiologia* **599**, 201–211.
 31. Torremorell, A., J. Bustingorry, R. Escaray and H. E. Zagarese (2007) Seasonal dynamics of a large, shallow lake, Laguna Chascomús: The role of light limitation and other physical variables. *Limnologia* **37**, 100–108.
 32. Torremorell, A., M. E. Llames, G. L. Pérez, R. Escaray, J. Bustingorry and H. Zagarese (2009) Annual patterns of phytoplankton density and primary production in a large, shallow lake: The central role of light. *Freshw. Biol.* **54**, 437–449.
 33. Pérez, G. L., A. Torremorell, J. Bustingorry, R. Escaray, P. Pérez, M. Diéguez and H. Zagarese (2010) Optical characteristics of shallow lakes from the Pampa and Patagonia regions of Argentina. *Limnologia* **40**, 30–39.
 34. Dangavs, N. V., A. M. Blasi and D. O. Merlo (1996) Geoliminología de la laguna Chascomús. *Revista Museo La Plata (NS). Geologia*. **11**, 167–195.
 35. Allende, L., G. Tell, H. Zagarese, A. Torremorell, G. Pérez, J. Bustingorry, R. Escaray and I. Izaguirre (2009) Phytoplankton and primary production in clear-vegetated, inorganic-turbid, and algal-turbid shallow lakes from the pampa plain (Argentina). *Hydrobiologia* **624**, 45–60.
 36. Diovisalvi, N., G. Berasain, F. Unrein, D. Colautti, P. Fermani, M. E. Llames, A. M. Torremorell, L. Lagomarsino, G. Pérez, R. Escaray, J. Bustingorry, M. Ferraro and H. E. Zagarese (2010) Chascomús: Structure and functioning of a turbid pampean shallow lake. *Ecología Austral*. **20**, 115–127.
 37. APHA (1998) *Standard Methods for the Examination of Water and Wastewater*. Vol. 20, 1220 pp. American Publication Health Association, Washington, DC.
 38. Sharp, J. H., E. T. Peltzer, M. J. Alperin, G. Cauwet, J. W. Farrington, B. Fry, D. M. Karl, J. H. Martin, A. Spitz, S. Tugrul and C. A. Carlson (1993) Procedures subgroup report. *Mar. Chem.* **41**, 37–49.
 39. Shooter, D., R. J. Davies-Colley and J. T. O. Kirk (1998) Light absorption and scattering by ocean waters in the vicinity of the Chatham Rise, South Pacific Ocean. *Mar. Freshw. Res.* **49**, 455–461.
 40. Jerlov, N. G. (1976) *Optical Oceanography*. Elsevier, New York.
 41. Stedmon, C. A., S. Markager and H. Kaas (2000) Optical properties and signatures of chromophoric dissolved organic matter (CDOM) in Danish coastal waters. *Estuar. Coast. Shelf. Sci.* **51**, 267–278.
 42. Twardowski, M. S., E. Boss, J. M. Sullivan and P. L. Donaghay (2004) Modeling the spectral shape of absorption by chromophoric dissolved organic matter. *Mar. Chem.* **89**, 69–88.
 43. Trüper, H. G. and C. S. Yentsch (1967) Use of glass fiber filters for the rapid preparation of in vivo absorption spectra of photosynthetic bacteria. *J. Bacteriol.* **94**, 1255–1256.
 44. Mitchell, B. G. and D. A. Kiefer (1984) Determination of absorption and fluorescence excitation spectra for phytoplankton. In *Marine Phytoplankton and Productivity* (Edited by O. Holm-Hansen, L. Bilis, and R. Gilles), pp. 157–169. Springer, Berlin.
 45. Bricaud, A. and D. Stramski (1990) Spectral absorption of living phytoplankton and nonalgal biogenous matter: A comparison between the Peru upwelling area and the Sargasso Sea. *Limnol. Oceanogr.* **35**, 562–582.
 46. Kishino, M., M. Takahashi and N. Okami (1985) Estimation of the spectral absorption coefficients of phytoplankton in the sea. *Bull. Mar. Sci.* **37**, 634–642.
 47. Morrow, J. H., W. S. Chamberlin and D. A. Kiefer (1989) A two-component description of spectral absorption by marine particles. *Limnol. Oceanogr.* **34**, 1500–1509.
 48. Zhang, Y., M. Liu, M. A. Van Dijk, G. Zhu, Z. Gong, Y. Li and B. Qin (2009) Measured and numerically partitioned phytoplankton spectral absorption coefficients in inland waters. *J. Plankton Res.* **31**, 311–323.
 49. Bricaud, A., M. Babin, A. Morel and H. Claustre (1995) Variability in the chlorophyll-specific absorption coefficients of natural phytoplankton: Analysis and parameterization. *J. Geophys. Res.* **100**(13), 321–13.
 50. Kirk, J. T. O. and P. A. Tyler (1986) The spectral absorption and scattering properties of dissolved and particulate components in relation to the underwater light field of some tropical Australian fresh waters. *Freshw. Biol.* **16**, 573–583.
 51. Kirk, J. T. O. (1981) A Monte Carlo study of the nature of the underwater light field in, and the relationships between optical properties of, turbid yellow waters. *Aust. J. Mar. Freshw. Res.* **32**, 517–532.
 52. Ferrero, E., M. Eöry, G. Ferreyra, I. Schloss, H. Zagarese, M. Vernet and F. Momo (2006) Vertical mixing and ecological effects of ultraviolet radiation in planktonic communities. *Photochem. Photobiol.* **82**, 898–902.
 53. Utermöhl, H. (1958) Zur Vervollkommnung der quantitativen Phytoplankton-methodik. *Mitt. Int. Ver. Theor. angew. Limnol.* **9**, 1–38.

54. Venrick, E. L. (1978) How many cells to count? In *Phytoplankton Manual* (Edited by A. Sournia), pp. 167–180. UNESCO, Paris.
55. Hillebrand, H., C. D. Dürselen, D. Kirschtel, U. Pollinger and T. Zohary (1999) Biovolume calculation for pelagic and benthic microalgae. *J. Phycol.* **35**, 403–424.
56. Laurion, I., A. Lami and R. Sommaruga (2002) Distribution of mycosporine-like amino acids and photoprotective carotenoids among freshwater phytoplankton assemblages. *Aquat. Microb. Ecol.* **26**, 283–294.
57. Mantoura, R. F. C. and C. A. Llewellyn (1983) The rapid determination of algal chlorophyll and carotenoid pigments and their breakdown products in natural waters by reverse-phase high-performance liquid chromatography. *Anal. Chim. Acta* **151**, 297–314.
58. V.-Balogh, K., B. Németh and L. Vörös (2009) Specific attenuation coefficients of optically active substances and their contribution to the underwater ultraviolet and visible light climate in shallow lakes and ponds. *Hydrobiologia* **632**, 91–105.
59. Zhang, Y., B. Zhang, X. Wang, J. Li, S. Feng, Q. Zhao, M. Liu and B. Qin (2007) A study of absorption characteristics of chromophoric dissolved organic matter and particles in Lake Taihu, China. *Hydrobiologia* **592**, 105–120.
60. Ma, R., J. Tang, J. Dai, Y. Zhang and Q. Song (2006) Absorption and scattering properties of water body in Taihu Lake, China: Absorption. *Int. J. Remote Sens.* **27**, 4277–4304.
61. Duarte, C. M., S. Agustí and J. Kalff (2000) Particulate light absorption and the prediction of phytoplankton biomass and planktonic metabolism in northeastern Spanish aquatic ecosystems. *Can. J. Fish. Aquat. Sci.* **57**, 25–33.
62. Le, C., Y. U. Zha and D. Sun (2009) Specific absorption coefficient and the phytoplankton package effect in Lake Taihu, China. *Hydrobiologia* **619**, 27–37.
63. Ciotti, A. M. and A. Bricaud (2006) Retrievals of a size parameter for phytoplankton and spectral light absorption by colored detrital matter from water-leaving radiances at SeaWiFS channels in a continental shelf region off Brazil. *Limnol. Oceanogr. Methods* **4**, 237–253.
64. Qin, B. and Y. L. Zhang (2008) Optical properties of Lake Taihu and radiative transfer simulation. In *Lake Taihu, China*, Vol. 87 (Edited by H. J. Dumont), pp. 69–113. Springer, Netherlands.
65. Cao, W., Y. Yang, X. Xu, L. Huang and J. Zhang (2003) Regional patterns of particulate spectral absorption in the Pearl River estuary. *Chin. Sci. Bull.* **48**, 2344–2351.
66. Lagomarsino, L., G. L. Pérez, R. Escaray, J. Bustingorry and H. E. Zagarese (2011) Weather variables as drivers of seasonal phosphorus dynamics in a shallow hypertrophic lake (Laguna Chascomús, Argentina). *Fund. Appl. Limnol.* **178**, 191–201.
67. Llames, M. E., L. Lagomarsino, N. Diovisalvi, P. Fermani, A. M. Torremorell, G. Pérez, F. Unrein, J. Bustingorry, R. Escaray, M. Ferraro and H. E. Zagarese (2009) The effects of light availability in shallow, turbid waters: A mesocosm study. *J. Plankton Res.* **31**, 1517–1529.
68. Huisman, J., H. C. P. Matthijs, P. M. Visser, H. Balke, C. A. M. Sigon, J. Passarge, F. J. Weissing and L. R. Mur (2002) Principles of the light-limited chemostat: Theory and ecological applications. *Antonie van Leeuwenhoek* **81**, 117–133.
69. Aalderink, R. H., L. Lijklema and J. Breukelman (1985) Quantification of wind induced resuspension in a shallow lake. *Water Sci. Technol.* **17**, 903–914.
70. Cózar, A., J. A. Gálvez, V. Hull, C. M. García and S. A. Loiselle (2005) Sediment resuspension by wind in a shallow lake of Esteros del Iberá (Argentina): A model based on turbidimetry. *Ecological Modelling* **186**, 63–76.
71. Morel, A. and A. Bricaud (1981) Theoretical results concerning light absorption in a discrete medium, and application to specific absorption of phytoplankton. *Deep Sea Res.* **28A**, 1375–1393.
72. Cloern, J. E. (1987) Turbidity as a control on phytoplankton biomass and productivity in estuaries. *Cont. Shelf Res.* **7**, 1367–1381.
73. Loos, E. A. and M. Costa (2010) Inherent optical properties and optical mass classification of the waters of the Strait of Georgia, British Columbia, Canada. *Prog. Oceanogr.* **87**, 144–156.
74. Scheffer, M. (1998) *Ecology of Shallow Lakes*. Chapman & Hall, London.

Figure S1

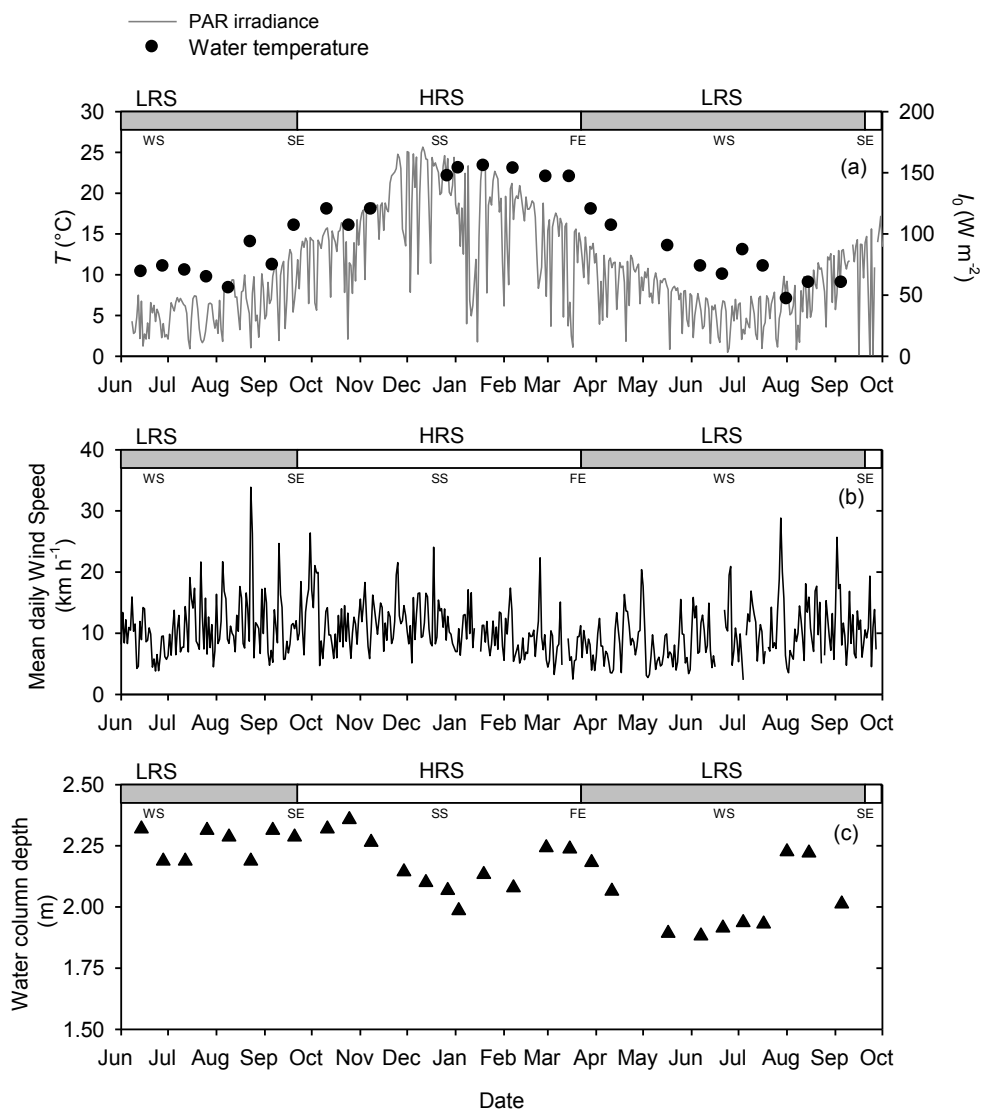


Figure S2.

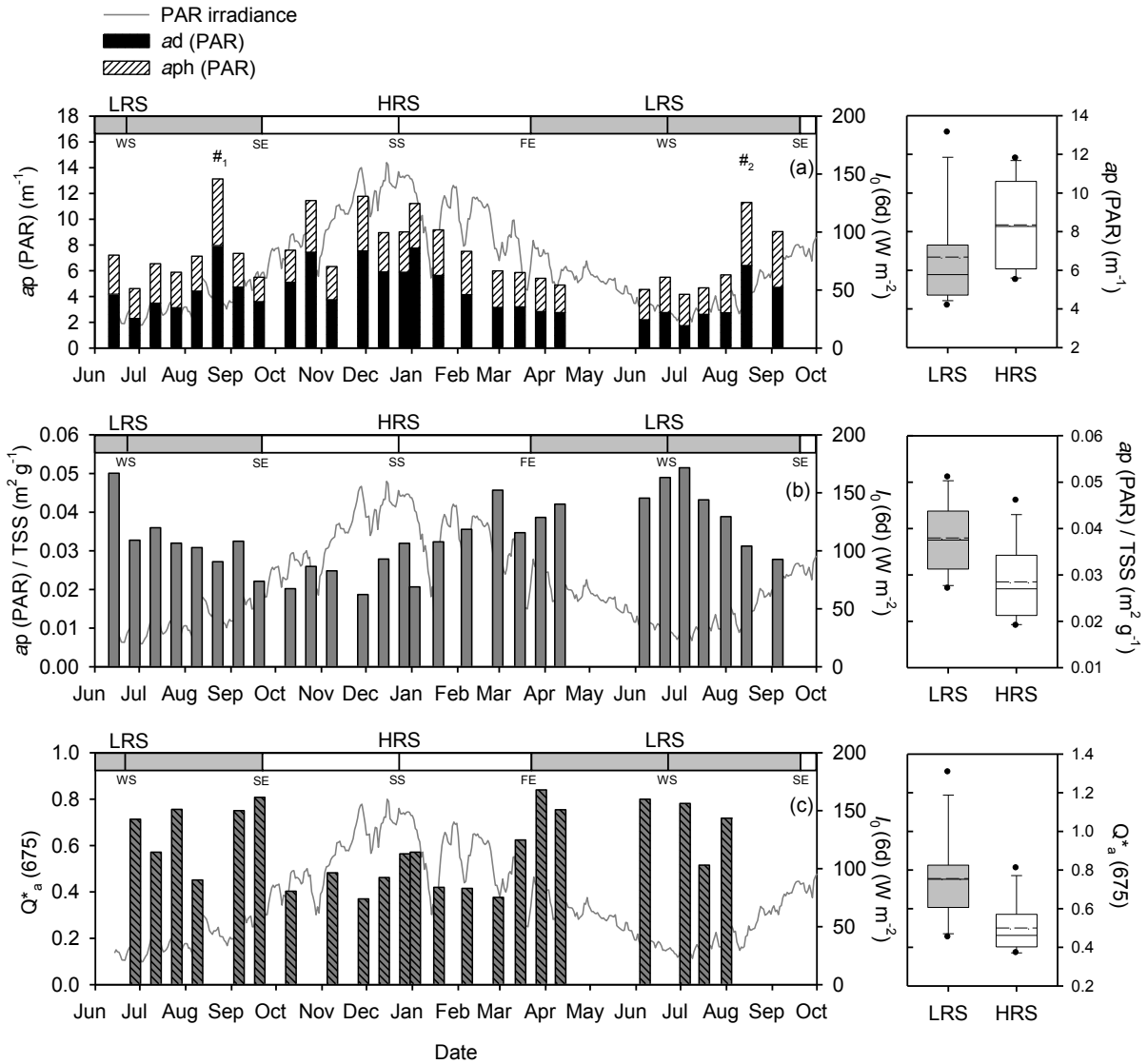


Figure S3.

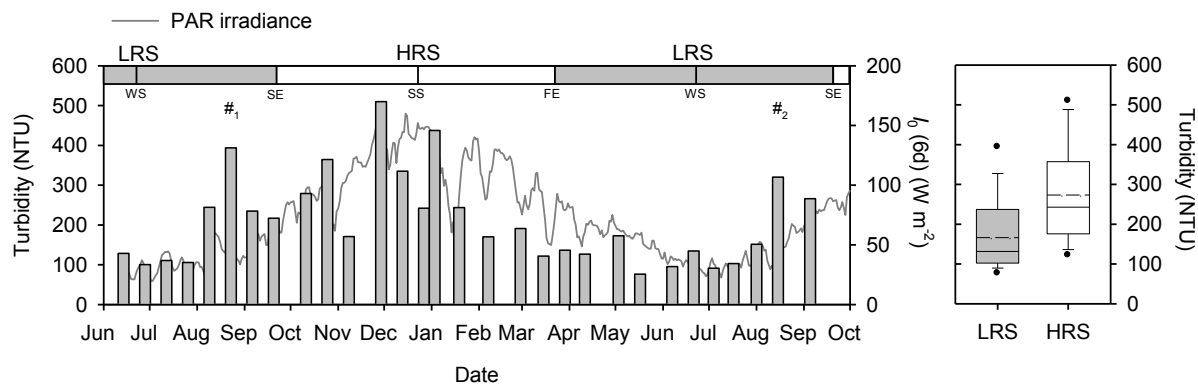


Figure S4.

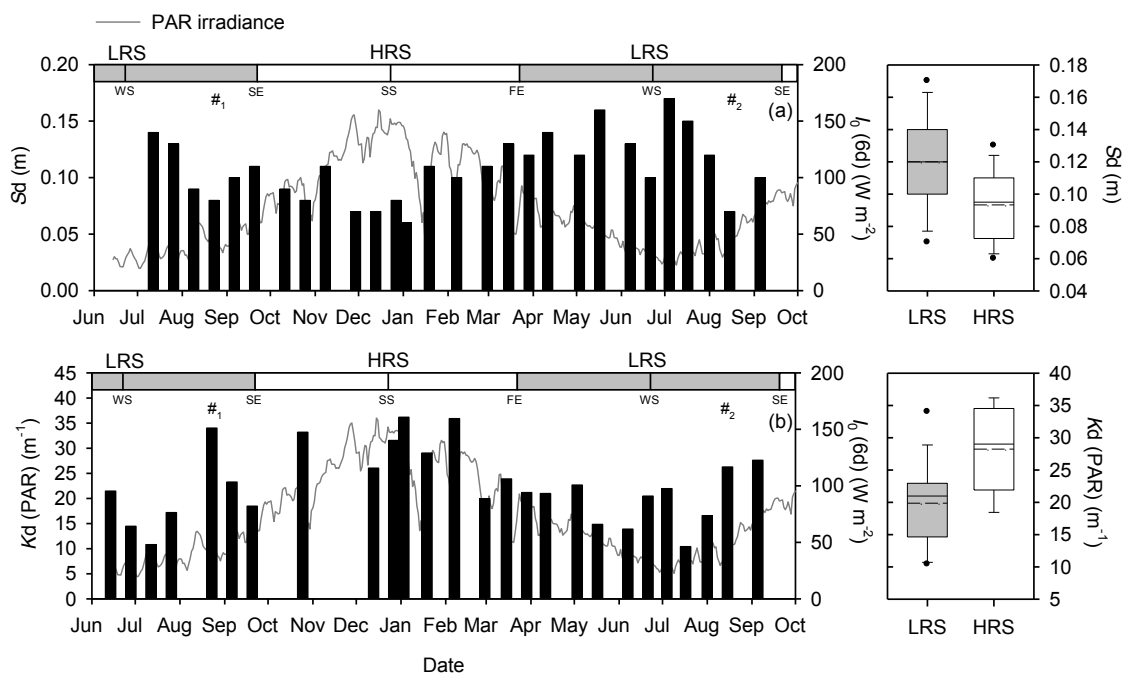


Table S1. Abbreviations of terms and variables used in the text.

NOTATION	
A	Absorbance (dimensionless) = Optical density
Acc. Pig.	Accessory pigments concentration ($\mu\text{g L}^{-1}$)
AFDW	Ash free dried weight (mg L^{-1})
$a_g(\lambda)$ and $a_w(\lambda)$	Spectral absorption coefficients of chromophoric dissolved organic matter and pure water (m^{-1})
$a(\text{PAR})$	Numerical mean absorption coefficient for PAR (m^{-1})
AOPs	Apparent Optical Properties
$a_p(\lambda)$, $a_d(\lambda)$ and $a_{ph}(\lambda)$	Spectral absorption coefficients of total particulate matter, nonalgal matter and phytoplankton (m^{-1})
$a_{ph}^*(\lambda)$	Spectral T-Chl <i>a</i> specific phytoplankton absorption coefficients ($\text{m}^2 \text{mg T-Chl } a^{-1}$)
Ash	Ash content (mg L^{-1})
$a_t(\lambda)$	Spectral total absorption coefficient (m^{-1})
$b(\lambda)$	Spectral scattering coefficient (m^{-1})
$\beta(\lambda)$	Pathlength amplification factor
CDOM	Chromophoric Dissolved Organic Matter
DOC	Dissolved organic carbon (mg L^{-1})
HRS	High radiation seasons (spring and summer)
I_0	Mean daily incident (24 h) irradiance at ground level (W m^{-2})
$I_0(6d)$	Mean incident irradiance between 1 to 6 days before sampling (W m^{-2})
IOPs	Inherent Optical Properties
$I_{z \text{ mean}}$	Mean irradiance in the water column (W m^{-2})
$K_d(\text{PAR})$	Vertical diffuse attenuation coefficient for PAR (m^{-1})
$K_{d_{\text{abs}}}(\text{PAR})$	Vertical attenuation coefficient assuming naught scattering
λ	Wavelength (nm)
LRS	Low radiation seasons (fall and winter)
OASs	Optically Active Substances
OPs	Optical Properties (i.e. apparent and inherent)
PAR	Photosynthetic Active Radiation
Q_a^*	The dimensionless efficiency factor for specific phytoplankton absorption
r	Pathlength of the optical cell (m)
s	The clearance area of the filter (m^2)
Sd	Secchi disk (m)
S_g	Spectral slopes of CDOM absorption coefficients.
T	Temperature ($^{\circ}\text{C}$)
T-Chl <i>a</i>	Total chlorophyll <i>a</i> concentration (Chl <i>a</i> + phaeophytin <i>a</i>) ($\mu\text{g L}^{-1}$)
T_n	Nephelometric turbidity (NTU)
TSS	Total suspended solids (mg L^{-1})
V	Volume of filtered water (m^3)
W	Mean daily wind speed (km h^{-1})
$W(9h)$	Mean wind speed form 9 h before sampling (km h^{-1})
Z_{eu}	Depth of the euphotic zone (m)
Z	Water column depth (m)